Electronic Supplementary Material (ESI) for ChemComm.

Electron-pair bonding in real space. Is the charge-shift family supported?

Electronic Supplementary Information.

J. L. Casals-Sainz, F. Jiménez-Grávalos, E. Francisco, A. Martín Pendás*

April 8, 2019

Contents

1 Basic Real Space Chemical bonding

Real space reasoning uses proper quantum mechanical observables to construct orbital invariant descriptors with chemical meaning. Among them, all reduced densities and density matrices (RDs, RDMs). An identification of spatial regions with chemical concepts is also necessary. This is usually done through spatial partitionings, normally induced by the topology of a scalar field. For instance, the topology of the electron density, ρ, induces an atomic partitioning: the Quantum Theory of Atoms in Molecules (QTAIM) explored by R. F. W. Bader and coworkers.[1] Similarly, the topology of Becke and Edgecombe's[2] electron localization function (ELF) provides a partition into cores, lone pairs and bonding domains, etc.

Once atoms (or electron-pair domains) are available, chemical bonding descriptors are built. Both the electron-counting perspective (leading to populations and bond orders) as well as the energetic view that provides bond strengths are needed. These are offered by, for instance, electron distribution functions (EDFs) and the interacting quantum atoms approach (IQA).

1.1 The energetic face of bonding: Interacting Quantum Atoms

Given an atomic spatial partitioning, the interacting quantum atoms (IQA) energy partition considers the one- and two-domain division of the non-relativistic Born-Oppenheimer electronic energy[3] described in the following equation,

$$\begin{aligned} E &= \sum_{\mathrm{A}} E^{\mathrm{A}}_{\mathrm{self}} + \sum_{\mathrm{A>B}} E^{\mathrm{AB}}_{\mathrm{int}} \\ &= \sum_{\mathrm{A}} T^{\mathrm{A}} + V^{\mathrm{AA}}_{\mathrm{ne}} + V^{\mathrm{AA}}_{\mathrm{ee}} + \sum_{\mathrm{A>B}} V^{\mathrm{AB}}_{\mathrm{nn}} + V^{\mathrm{AB}}_{\mathrm{ne}} + V^{\mathrm{BA}}_{\mathrm{ne}} + V^{\mathrm{AB}}_{\mathrm{ee}}, \end{aligned} \tag{1}$$

wherein $E^{\mathrm{A}}_{\mathrm{self}}$ and $E^{\mathrm{AB}}_{\mathrm{int}}$ are the IQA self and interaction energies of atom A and pair AB, while T^{A} denotes the kinetic energy of atom A. Finally, the terms $V^{\mathrm{AB}}_{\mathrm{ne}}$ and $V^{\mathrm{AB}}_{\mathrm{ee}}$ stand for (i) the attraction between the nucleus of domain A and the electrons of atom B and (ii) the repulsion between the electrons in atom A with those in basin B, respectively.

We can get further insight about the nature of the interaction between two atoms by separating the electronic repulsion into its Coulombic and exchange-correlation components. This splitting allows, in turn, the separation of the IQA interaction energy of a pair AB as[3]

$$E_{\rm int}^{\rm AB} = V_{\rm cl}^{\rm AB} + V_{\rm xc}^{\rm AB} = E_{\rm ion}^{\rm AB} + E_{\rm cov}^{\rm AB}. \tag{2}$$

Usually binding is measured relative to appropriate reference for the quantum fragments A, with $E^{A,0}$. Then $E^A_{self} - E^{A,0} = E^A_{def}$ is called the atomic or fragment deformation energy, which corresponds to a combination of the traditional promotion energy and other effects, like spin-recoupling, true electronic deformation, etc.[4] We have shown that the IQA interaction energies behave as *in situ* bond energies. IQA thus provides an invariant decomposition of the energy into group deformations and bond contributions in which covalent and ionic energies acquire rather pure forms.

1.2 The electron-counting face of bonding: Electron Distribution Functions

Electron counting provides access to the more qualitative view of chemical bonding in which the number of electrons engaged in sharing or in pure transfer between atoms gives rise to bonding descriptors like bond orders. In real space we simply examine the distribution of the electron population in the atomic regions in which we have divided the space.

EDFs are defined as follow. Given an N–electron molecule and an exhaustive partition of the real space ($\mathcal{R}^3$) into m arbitrary regions Ω_1, Ω_2, ..., Ω_m ($\Omega_1 \cup \Omega_2 \cup \cdots \cup \Omega_m = \mathcal{R}^3$), an EDF is the distribution function formed by all the probabilities $p(n_1, n_2, \ldots, n_m)$ of finding exactly n_1 electrons in Ω_1, n_2 electrons in Ω_2, ..., and n_m electrons in Ω_m, $\{n_p\}$ being integers ($n_i \in \mathcal{N}$) satisfying $n_1 + n_2 + \cdots + n_m = N$. This view is in accord with considering subsystems as open quantum systems in which number operators do not commute with the subsystem hamiltonian. In this way, Ψ is not an eigenstate of the operator defining the number of electrons in domain Ω_i, $\hat{N}_{\Omega_i}$. This means that the average number of electrons in Ω_i is not an eigenvalue of $\hat{N}_{\Omega_i}$, so that measuring the number of electrons in the domain will render values n_{Ω_i} ranging from 0 to N, the total number of electrons, with a defined set of probabilities, $p(n_{\Omega_1})$. This is the one-fragment EDF for domain Ω_i. To obtain these probabilities or, in general, the multivariate

electron distribution functions $p(n_1, n_2, \cdots, n_m)$, one needs $\Psi(1, \ldots, N)$, Ψ being the complete wave function,

$$p(n_1, n_2, \ldots, n_m) = N!\Lambda \int_D \Psi^\star \Psi d\mathbf{x}_1 \cdots d\mathbf{x}_N, \tag{3}$$

where D is a multidimensional domain in which the first n_1 electrons are integrated over Ω_1, the second n_2 electrons over Ω_2, $\cdots$, and the last n_m electrons over Ω_m, and $N!\Lambda = N!/(n_1!n_2!\cdots n_m!)$ is a combinatorial factor that accounts for electron indistinguishability. The 3D domains of these integrations can be arbitrary, but when using QTAIM atomic basins, a partition of the N electrons of the molecule that assigns a given number of electrons (including possibly 0) to each of these regions will was called a *real space resonance structure* (RSRS)[5] and there are $N_S = (N + m - 1)!/[N!(m - 1)!]$ of these for a given N,m pair. With the notation $S(n_1, n_2, \ldots, n_m) \equiv S(\{n_p\})$, or simply $(n_1, n_2, \ldots, n_m) \equiv \{n_p\}$, we label the resonance structure having n_1 electrons in Ω_1, n_2 electrons in Ω_2, ..., and n_m electrons in Ω_m. If electrons are spin-seggregated, then we come to spin-resolved EDFs, and a set of probabilities $p(n_1^\alpha, n_1^\beta, n_2^\alpha, n_2^\beta, \ldots, n_m^\alpha, n_m^\beta)$ which gives extremely fine-grained information about how electrons and their spins distribute.[6]

The computation of $p(n_1, n_2, \ldots, n_m)$ for all the RSRSs provides all the statistical moments of the electron populations, including the average number of electrons in a given region, or its fluctuation. The average population is obviously given by

$$N_i = \langle n_i \rangle = \sum_{\{n_p\}} n_i \times p(\{n_p\}) = \sum_{n_i} n_i p_i(n_i). \tag{4}$$

It is not difficult to show that the number of shared pairs between two regions may be obtained directly by counting the number of intra- and interpairs.[7] This has given rise to the so-called localization and delocalization indices, $(\lambda^{ii}, \delta^{ij})$, which determine the number of *localized* and *delocalized* pairs. The latter, which is the covalent bond-order in real space can be obtained from the $p(\{n_p\})$ probabilities as

$$\delta^{ij} = -2\mathrm{cov}(i,j) = -2\left[\langle n_i n_j\rangle - \langle n_i\rangle\langle n_j\rangle\right] = \tag{5}$$

$$-2\left[\sum_{\{n_p\}} n_i n_j \times p(\{n_p\}) - \langle n_i\rangle\langle n_j\rangle\right] = \tag{6}$$

$$-2\sum_{n_i n_j}(n_i - N_i)(n_j - N_j)p(n_i, n_j) = 2N_{ij} \tag{7}$$

where the -2 factor has been included to comply with the usual definition of δ in terms of the exchange-correlation density and to ensure that the bond order for an ideal single bond is equal to 1,

$$\delta^{ij} = -2\int_{\Omega_i}\int_{\Omega_j} d\boldsymbol{x}_1\; d\boldsymbol{c}_2\rho_{xc}(1,2). \tag{8}$$

The localization index is given by

$$\lambda_{ii} = N_i - \mathrm{cov}(i,i) = N_i - var(i) = N_i - \sum_{n_i}(n_i - N_i)^2 p(n_i) = N_{ii} \tag{9}$$

From equations 5-9 it is clear that $N_{ii} = N_i$ if the variance is zero and that $N_{ij} = 0$ if the covariance is cero. This is the starting point for a complete theory of chemical bonding based on the fluctuation of electron populations. There is chemical bonding between two regions if their electron populations are not statistically independent. A sum rule, that classifies electrons into localized and delocalized sets appears:

$$N = \sum_{\Omega_i} N_i = \sum_{\Omega_i}\lambda^{ii} + \frac{1}{2}\sum_{\Omega_i\neq\Omega_j}\delta^{ij}. \tag{10}$$

Suitable generalizations in the case of multi-center bonding exist.[8]

1.3 Natural Adaptive Orbitals

We have shown in the last years that the use of further order reduced density matrices (RDMs) and real space partitions can be used to derive a hierarchical set of general bonding indices.[9] The key objects are found to be the n-th

order cumulant density matrices (nCDMs), which convey information about true n-body correlations.

As in statistics, it is legitimate to extract from the n-th order RDMs those parts that contain true n-particle correlations, i.e., those parts that cannot be written in terms of lower order RDMs. This is provided by the so-called cumulant densities or cumulant density matrices. With them, n-center chemical bonding is the result of simultaneous n-center fluctuation of electron populations.

In this general scheme, n-center bonding indices and a set of one electron functions for each, that we called natural adaptive orbitals (NAdOs), are obtained by domain-averaging appropriate CDMs. General n-NAdOs describe n-center bonds in real space (or cores and lone pairs, if $n = 1$). NAdOs are adaptively localized or delocalized orbitals over the n centers in which they have been computed, and only those which are at least partly localized in the chosen n-center regions contribute to n-center bonding. Coming from invariant RDMs, NAdOs are also invariant under orbital transformations, as standard natural orbitals.

Domain averaging nCDMs provides the entry point to introducing chemical bonding descriptors that are generalizations of those used in standard MO theory. If all but one electron coordinate in the nCDM is averaged over a domain, an n-center decomposition of the electron density, $\rho = \rho^1_C$, appears as

$$\rho(r) = \sum_{ab\ldots n} \rho^1_{ab\ldots n} = \tag{11}$$

$$\sum_{ab\ldots n} \int_{\Omega_a} dr_2 \int_{\Omega_b} dr_3 \cdots \int_{\Omega_n} dr_{n+1}\ \rho^{n+1}_C(r, r_2, \ldots, r_{n+1}), \tag{12}$$

where ρ^n_C is the nCD. It can be shown[8] that $\rho^1_{ab\ldots n}$ may be written in terms of the occupied MOs of the system as

$$\rho^1_{ab\ldots n} = \phi(r) D^{ab\ldots n} \phi^\dagger(r), \tag{13}$$

where ϕ is a vector comprising all the occupied orbitals and D a hermitian matrix. Upon diagonalization of the above expression,

$$\rho^1_{ab\ldots n} = \sum_i n_i^{ab\ldots n} |\psi_i^{ab\ldots n}|^2, \tag{14}$$

we obtain the multi-center NAdOs $\psi^{ab...n}$ and their natural adaptive occupation numbers (NAdOccs). The NAdOccs fulfil the sum rule $\sum_i n_i^{ab...n} = \langle N_{ab...n} \rangle$, so that NAdOs induce a one-electron decomposition of any multi-center delocalization index. In the $n = 2$ case, the covalent bond order is partitioned into a set of eigencomponents.

NAdOs and NAdOccs can be immediately interpreted. If a 2-NAdO is completely localized its occupation (contribution to the bond order) vanishes, and when it is equally shared it peaks to 1 if the link is uncorrelated. NAdOccs may easily be used to uncover both polarity and covalency. We also refer to them as eigencomponens of the delocalization index.

1.4 2c-2e bonds

The statistical link between the fluctuation of electron populations and the standard energetic and bond order descriptors allows to map all coarse-grained (i.e. condensed at the atomic level) possible $(2c-2e)$ bonds through simple models. In a two-center, two-electron system there are only three RSRSs: $(2,0)$, $(1,1)$, $(0,2)$, where we label how many electrons lie in each of the a, b domains. The EDF space is two-dimensional, since $p(2,0)+p(1,1)+p(0,2) = 1$, and all bond indices become fully mapped in this 2D space. A convenient coordinate system can be built with the probability that any of the electrons lie in one of the basins, e.g. the left one, which we call p and provides a measure of heteropolarity, and a correlation factor $-1 \leq f \leq 1$ that determines how the electronic motion is correlated. $f = 1$ means that an electron is completely excluded from one domain if the other is already in it (positive correlation) and $f = -1$ implies that the two electrons are always found together within the same domain (negative correlation). The correlation factor here defined plays the same role as that used in density matrix theory, where $\rho^2(r_1, r_2) = \rho(r_1)\rho(r_2)(1-f)$. The (p, f) pair describes fully a 2c,2e link at this level: $p(2,0) = p^2 - p(1-p)f$, $p(1,1) = 2p(1-p)(1+f)$ and $p(0,2) = (1-p)^2 - p(1-p)f$.[10]

If we use these p, f parameters, the covalent bond order becomes $\delta = 4p(1-p)(1-f)$. An ionic bond order $\iota = -Q_a Q_b$ where Q is the net charge of a center has also been defined.[11] In standard weakly correlated bonds with positive $f \sim 0$, the EDF is close to binomial, and δ peaks at $\delta = 1$ for a purely covalent homopolar link with $p = 1/2$. As electron correlation, f , or polarity, p, increases δ decreases. Moreover, for non-correlated links with $f = 0$ $\iota = 1 - \delta$ so, in agreement with standard wisdom, the ionic and

covalent bond orders are inversely correlated.

When f deviates from zero, the model describes positively or negatively correlated bonds. The latter case implies a bosonization of the link. Electrons try to delocalize together, giving rise to very large fluctuations. The most extreme 2c,2e case with $\delta = 2$ occurs when $p(0,2) = p(2,0) = 1/2$ and $p(1,1) = 0$, i.e. when there is a resonance between the two non-orthogonal valence bond (NOVB) ionic structures. Thus, $f < 0$ serves to separate cleanly, in real space, large fluctuations from the standard bonding regime.

Several rigorous bond-energy bond-order (BEBO)[11] relations can be uncovered using these real space descriptors. Under the IQA perspective a multipolar expansions shows that the first order ionic and covalent energies are immediately related to their corresponding bond orders. For an interaction between atoms A and B,

$$E_{ion}^{AB} \sim -\frac{\iota^{AB}}{R_{ij}} \quad E_{cov}^{AB} \sim -\frac{1}{2}\frac{\delta^{AB}}{R_{AB}}. \tag{15}$$

2 The two-state model

A two-center (A,B) homonuclear electron-pair link is assumed, both in Heitler-London-like and orthogonal descriptions. Two localized functions a and b with $\langle a|b\rangle = S$ are used. In the VB framework, the basis is

$$\begin{aligned}
\Psi_{cov} &= \frac{1}{\sqrt{2(1+S^2)}}(a(1)b(2)+b(1)a(2))\frac{1}{\sqrt{2}}(\uparrow\downarrow+\downarrow\uparrow), \\
\Psi_{ion} &= \frac{1}{\sqrt{2(1+S^2)}}(a(1)a(2)+b(1)b(2))\frac{1}{\sqrt{2}}(\uparrow\downarrow+\downarrow\uparrow).
\end{aligned} \tag{16}$$

Similarly, the MO basis is formed from the *gerade* and *ungerade* combinations

$$g = \frac{1}{\sqrt{2(1+S)}}(a+b),\ u = \frac{1}{\sqrt{2(1-S)}}(a-b), \tag{17}$$

so that two independent, orthogonal MO states are:

$$\Psi_{gg} = \Psi_{\mathrm{HF}} = |g\bar{g}|,\ \Psi_{uu} = |u\bar{u}|. \tag{18}$$

Inactive electrons are added as needed to form a proper antisymmetric multi-electron function. In general,

$$\Psi = c\Psi_{cov} + i\Psi_{ion} = \lambda\Psi_{gg} + \mu\Psi_{uu}. \tag{19}$$

Figure 1: Pictorial representation of the parameters of the λ, μ model. The ω angle at which the c, i structures are met depends on the overlap S. If $S = 0$, $\omega = \pi/2$.

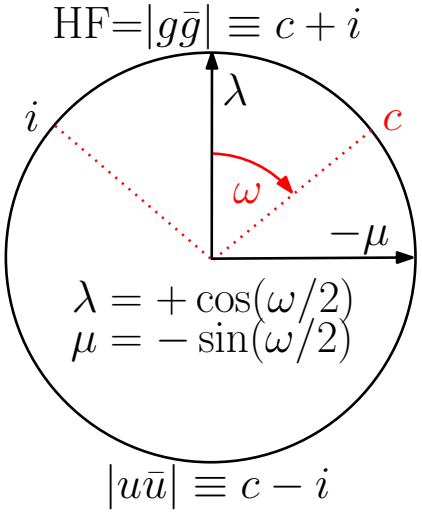

The $\lambda^2 + \mu^2 = 1$ condition allows to map easily the full spectrum of the two-state model by using a ω-angle polar representation such that $\lambda = \cos(\omega/2)$, $\mu = -\sin(\omega/2)$, $\omega \in [-\pi, \pi]$. Moreover, if the coefficients $\alpha = \lambda/(2+2S)$ and $\beta = \mu/(2-2S)$ are defined, then it is easily shown that $\alpha + \beta \propto i$, $\alpha - \beta \propto c$, and that the HL covalent structure is obtained when $\alpha = -\beta$ and the ionic one when $\alpha = \beta$, implying that the VB ionic structure is found in the (λ, μ) map by simply changing the sign of either λ or μ from their values at the VB covalent structure: $(\lambda_i, \mu_i) = (\lambda_c, -\mu_c)$, for instance. If a positive λ value is forced, then it is usually found that the minimum energy CAS[2,2] solution has negative μ. Being this normally closer to the VB covalent structure, the state that mimics the VB ionic structure has positive μ value. In the following, as shown in the main paper, the CAS solution is found and its orbitals are fixed. The approximate (λ, μ) pairs for the covalent and ionic structures are obtained from the orbital overlap, since $\lambda^2 = (1+S)^2/(2+2S^2)$. The map is sketched in Fig. 1

Working in the orthogonal λ, μ representation provides direct easy access to all reduced density matrices. Since the $|g\bar{g}|$ and $|u\bar{u}|$ determinants differ

in two spinorbitals, only the 2RDM has coupling terms,

$$\begin{aligned}\rho(\boldsymbol{r};\boldsymbol{r}') &= 2\lambda^2 g(\boldsymbol{r})g(\boldsymbol{r}') + 2\mu^2 u(\boldsymbol{r})u(\boldsymbol{r}') \\ \rho_2(\boldsymbol{r}_1,\boldsymbol{r}_2) &= 2\lambda^2 g^2(\boldsymbol{r}_1)g^2(\boldsymbol{r}_2) + 2\mu^2 u^2(\boldsymbol{r}_1)u^2(\boldsymbol{r}_2) + 2\lambda\mu\ gu(\boldsymbol{r}_1)gu(\boldsymbol{r}_2)\end{aligned} \quad (20)$$

All one-electron properties vary linearly with λ^2 between the Hartree-Fock and the $|u\bar{u}|$ values. At the bond critical point (bcp) which lies at the center of the internuclear axis, both $\rho, \nabla^2\rho = \lambda^2 G + (1-\lambda^2)U$, where G, U are their values in the gg and uu determinants. Since for any scalar function f, $\nabla^2 f^2(\boldsymbol{r}) = 2\boldsymbol{\nabla} f(\boldsymbol{r}) \cdot \boldsymbol{\nabla} f(\boldsymbol{r}) + 2f(\boldsymbol{r})\nabla^2 f(\boldsymbol{r})$, and $u_{bcp} = 0$, $g_{bcp} \neq 0$,

$$\begin{aligned}\nabla^2 g_{bcp}^2 &= 2g_{bcp}\nabla^2 g_{bcp} \approx 8a_{bcp}\nabla^2 a_{bcp}, \\ \nabla^2 u_{bcp}^2 &= 2|\nabla u_{bcp}|^2 \approx 8|\nabla a_{bcp}|^2 > 0.\end{aligned} \quad (21)$$

At the bcp, ρ decreases linearly with $\mu^2 = 1-\lambda^2$ from $2g_{bcp}^2$ to 0. Using an exponential ansatz, $a \approx Ne^{-}\zeta r$, $\nabla^2 g_{bcp}^2 \approx 8N^2 e^{-2\zeta r}(\zeta^2 - 2\zeta/r)$, and $\nabla^2 u_{bcp}^2 \approx 8N^2 e^{-2\zeta r}\zeta^2$, so $\nabla^2\rho$ increases with λ, μ mixing. Since standard homolytic dissociation increases mixing, the laplacian tends to be more positive for a proto-covalent bond. Moreover, at large distances, the $\nabla^2 a$ term tends also to a positive value. Positive laplacians appear necessarily upon homolytic bond dissociation.

2.1 The two-state model (TSM) in the H_2 molecule

The dihydrogen molecule is hereby used as an example. A calculation in the minimal STO-6G basis set provides $\lambda^2 = 0.987$, $S = 0.681$, so that for the VB covalent structure with CAS fixed orbitals, $\lambda_c^2 = 0.965$. A straightforward calculation gives $V_{ee}^{uu} = 0.699$ au, $V_{ee}^{gg} = 0.675$ au, so that $\langle gu|r_{12}^{-1}|gu\rangle = 0.182$. Fig. 2 shows how the total one-electron energy components favor the HF solution, so that (with fixed orbitals) it is the too large electron repulsion of the HF state the term responsible for λ, μ mixing. Given the scales of the 1e and 2e energy variations with the ω angle, the CAS solution is very close to the HF one. From the VB point of view, the covalent and ionic states share the same 1e-terms, and only differ in the V_{ee} repulsion. The covalent state displays a not stabilizing enough 1e energy (too large kinetic energy in standard reasoning) and the mixing decreases it at the expense of rising the total V_{ee}. Notice that it is the electron repulsion which puts a brake on the degree of mixing. Without it, the system would collapse onto the Hartree-Fock state.

Figure 2: Variation of the 2e-energy (top) and of the 1e and total energy (bottom) of the STO-6G dihydrogen molecule with CAS[2,2] fixed orbitals.

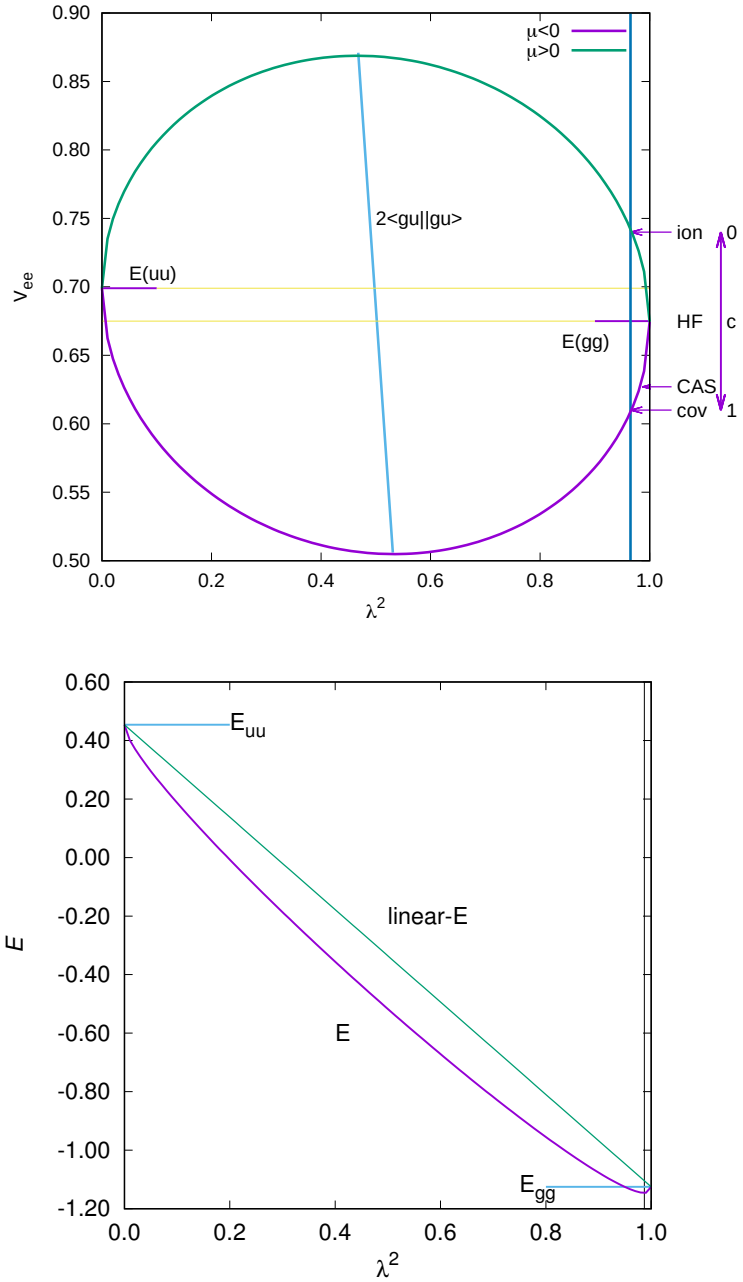

Table 1: Total energy components for several 6-31G* states in H_2 with fixed CAS[2,2] orbitals at $R_e = 1.40$ au. All data in au. $\lambda_c \approx 0.98$ estimated from S.

Ψ	E	T	V_{ne}	V_{ee}
uu	0.413	3.050	-4.036	0.697
ion	-1.012	1.202	-3.367	0.721
gg	-1.131	1.133	-3.622	0.655
CAS	-1.150	1.156	-3.619	0.619
cov	-1.139	1.202	-3.367	0.594

A still simple 6-31G* calculation in H_2 in which the λ_c is estimated from the overlap integral $S \approx 0.70$ provides the following parameters, gathered in Table 1. All the insights previously commented are fully supported. If we take the λ, μ point of view, then a non-zero μ value decreases V_{ee} while increasing the 1e energy. From the VB one, mixing the covalent with the ionic structure decreases the too large 1e energy until V_{ee} puts a stop. Notice how the interpretation can be rather different depending on the starting point. If we begin with a mean-field HF solution, the gg determinant displays too large V_{ee} and (λ, μ) mixing decreases it at the expense of increasing the kinetic energy. The contrary occurs when our starting point is the VB covalent structure. In both cases, it is the non-linear behavior of V_{ee} which acts as a controlling factor.

2.2 TSM in the F_2, N_2 and O_2 molecules

A CAS[2,2]//6-31G* calculation in difluorine with an active space composed of the $2p_z$ σ, σ^* set provides $R_e \approx 1.49$ Å. and $D_e \approx 16$ kcal/mol. A much smaller S leads to $\lambda_c \approx 0.80$. As stated in the main text (Table 2), now the 1e electron energy is smaller in the uu than in the gg determinant. This implies that the slope of the linear part in the bottom panel of Fig. 2 is reversed. The reversal is not due to the kinetic energy part, that is obviously minimum at the gg determinant, but to the electron-nucleus attraction, which becomes strongly stabilizing as the density is compacted by (λ, μ) mixing. As shown in the main text, it is again V_{ee}, actually the active-core repulsion, which avoids the collapse onto the uu solution.

We have performed similar σ, σ^* CAS[2,2] 6-31G* calculations in N_2 and O_2. In the former, $R_e = 1.08$ Å with $\lambda = 0.9986$, while in the latter $R_e = 1.18$

Table 2: Total energy components for several 6-31G* states in N_2 and O_2 with fixed CAS[2,2] orbitals at the theoretical equilibrium geometry. All data in au.

N_2	E	T	V_{ne}	V_{ee}	O_2	E	T	V_{ne}	V_{ee}
gg	-108.944	108.555	-303.343	61.895	gg	-149.597	149.102	-411.924	84.401
CAS	-108.956	108.578	-303.361	61.878	CAS	-149.622	149.790	-411.990	84.467
uu	-105.076	116.559	-309.510	63.926	uu	-147.199	155.712	-418.569	86.925

Table 3: Relevant IQA data in 6-31G* F_2 at $R = 1.2$ au with $\lambda_c \approx 0.8$. All data in au and all orbitals fixed to those in the CAS.

F_2	E^A_{def}	T^A	V^{AA}_{ee}	E^{AB}_{int}	E^{AB}_{cov}	V^{AB}_{ee}	δ^{AB}
cov	0.254	100.481	41.164	-0.072	-0.225	33.015	0.633
CAS	0.138	99.491	40.846	-0.245	-0.388	32.884	1.128
HF	0.191	98.421	40.885	-0.307	-0.450	32.825	1.366
ion	0.707	100.481	41.617	-0.443	-0.595	32.644	2.148

Å. with $\lambda = 0.9950$. Table 2 summarizes the results. It can be readily checked that dinitrogen belongs to the H_2 family, so that the 1e energy is minimum for the mean-field solution, while in O_2 and F_2 the contrary is true. As explained in the main text, it is the core-active interelectron repulsion which increases steeply from the gg to the uu determinants, pointing toward traditional LPBWE.

2.3 The role of the internuclear distance in F_2

In order to understand why larger than expected internuclear distances are found in CSB we have also analyzed our model upon compression. Table 3 gathers 6-31G* IQA results for difluorine at $R = 1.2$ au, and should be compared with Table 3 in the main text. At this compressed distance, all the effects become magnified: the covalent solution has now larger deformation energy than even the Hartree-Fock one, with a kinetic energy 1 E_h in excess with respect to the CAS solution. Moving from either the covalent or the HF states to the CAS minimum decreases considerably the deformation energy as well as V^{AA}_{ee}, exactly as at the equilibrium geometry.

We think it is rather relevant to point out that even at this compressed distance the covalent structure is rather unable to delocalize effectively its

Table 4: Non-negligible EDF probabilities in 6-31G* F_2 with orbitals and distances fixed to those in the CAS solution. CAS(2e) refers to the active orbital subsystem.

RS	cov	CAS	CAS(2e)	ion
(9,9)	0.735	0.684	0.748	0.175
(10,8)	0.135	0.151	0.126	0.374

electrons. The delocalization index is only 0.63. This lies at the root of the large NOVB covalent-ionic mixing: the compact localized VB orbitals lead to small delocalization and large LPBWE repulsion which is ameliorated by mixing. As previously noticed,[12] a similar mixing effect can be forced in dihydrogen if too compact orbitals are used. Shifting to the CAS solution δ increases to 1.13. Nevertheless, the c, i mixing does not lead to the purported electron-pair fluctuation, as shown by the small $p(2,0)$ probability. Table 4 shows the EDF for the covalent, CAS, and ionic TSM structures in difluorine. Both the CAS and covalent results show smaller fluctuation than a standard link.

Notice that the full EDF is related to the VB structure weights, although the non-zero overlap of the VB covalent and ionic structures introduces some non-linearity. Overall, the VB-covalent and VB-ionic weights in dihydrogen and difluorine are rather similar,[12] and disregarding non-linearities, so are their EDFs. This clearly shows (high level calculations below do not change the scenario) that electron-pair fluctuations in CSB systems like difluorine are not larger than in normal covalently linked moieties. The CSB literature[12] substantiates part of the CSB singularity in these fluctuations, which have computed through the variance of the electron population in ELF basins. As commented in the main text, these data are unreliable since they were obtained using DFT pseudo second-order densities. In our opinion, even trusting these numbers beyond what it should be acceptable, the variances of ELF basins in CSBs are not larger than those found in other systems: they are simply comparable to the total ELF basin populations, which are very small in CSBs. This behavior is interesting (and needs to be corroborated through exact variance calculations), but does not provide an absolute measure of larger than normal fluctuation, it just shows that the relative fluctuation is larger. Moreover, if the pair fluctuates, it is necessary that its two-electrons be located at some point in one of the atomic regions, something that should impact the EDF.

We have recently shown[13] that care has to be taken to understand the meaning of VB structure coefficients in real space. Very succinctly, electron delocalization, that drives covalent interactions, is related to the amount of $(2,0)$ and $(0,2)$ EDF weights, i.e. to the amount of VB-like ionic contributions. Without them, there is no homonuclear bonding. Due to the compactness of the electron distributions in many CSB systems, the VB covalent structure has not sufficient real-space ionic $(2,0)-(0,2)$ contributions, as Table 4 shows, and does not bind due to the large intra-atomic deformations. This problem is overcome after the VB-cov mixes with the VB-ion structure.

In the end, a similar EDF is found both in dihydrogen and difluorine, with similar interatomic IQA energetics and very different IQA (intra-atomic) deformation energies.

3 Beyond the TSM

Although we think that the two-state model contains the basic physics behind the large NOVB covalent-ionic resonance energies found in CSB, the real space artillery can be actually applied to high-level correlated calculations, from perturbative approaches like MP2, to CCSD(T).[14] To obtain EDFs, however, a determinant based approach is needed, so that we have decided to perform large-space multiconfigurational calculations on a series of already reported CSB molecules, see Tables 5 and 6.

Calculations were done as follows. For all systems we have used CASSCF selecting as configuration interaction solver the heat bath method.[22–24] Although some dynamical correlation is still lacking in such a description, this provides a limited set of determinants to perform EDF calculations, without affecting seriously the conclusions. In all cases a criterion of 8×10^{-5}H was used for the selection criteria. In the case of Au_2 and $Hg_2{}^+$, scalar relativistic corrections were used at the X2C level,[25] using the totally decontracted basis. The active space was selected using a modified AVAS[26] procedure, where a defined set of core orbitals are excluded from the projection step and a splitting of the threshold for the occupied and virtual sets, 0.1, 10^{-5} respectively for non metals and 0.01, 10^{-5} for the rest was implemented in order to achive better active spaces. Details of geometries and active spaces are found in table 5. In all cases the Sapporo-QZP-2012 basis set[18] with diffuse basis functions was used, and the corresponding relativistic bases when

Table 5: AVAS active space and details for molecules studied in this work. A threshold of 0.1 au was used for the occupied space and 1×10^{-5} au for the virtual space.

Molecule	Distance(Å)	State	Core	Impurities	Active Space
H_2	0.7414[15]	$^1\Sigma_g^+$	0	1s,2s,2p	2e,11o
C_2	1.2425[15]	$^1\Sigma_g^+$	2	2s,2p,3s,3p	8e,20o
N_2	1.0976[15]	$^1\Sigma_g^+$	2	2s,2p,3s,3p	10e,21o
N_2H_4	1.4459[15]	$^1\Sigma^+$	2	2s,2p,3s,3p	14e,23o
O_2	1.2075[15]	$^3\Sigma_g^-$	2	2s,2p,3s,3p	12e,23o
H_2O_2	1.4749[15]	$^1\Sigma^+$	2	2s,2p,3s,3p	14e,23o
F_2	1.4119[15]	$^1\Sigma_g^+$	2	2s,2p,3s,3p	14e,23o
S_2	1.8899[15]	$^3\Sigma_g^-$	10	3s,3p,4s,4p	12e,23o
Cl_2	1.9879[15]	$^1\Sigma_g^+$	10	3s,3p,4s,4p	14e,23o
Br_2	2.2810[15]	$^1\Sigma_g^+$	28	4s,4p,5s,5p	14e,23o
Cu_2	2.2200[16]	$^1\Sigma_g^+$	18	4s,4p,5s,5p	10e,21o
Ag_2	2.5300[16]	$^1\Sigma_g^+$	36	5s,5p,6s,6p	10e,21o
Au_2	2.4700[16]	$^1\Sigma_g^+$	54	6s,6p,7s,7p	16e,24o
Hg_2^+	2.6988[17]	$^1\Sigma_g^+$	54	6s,6p,7s,7p	12e,22o
Propellane	1.5960[15]	$^1A_1$	5	C1,C5,2s,2p,3s,3p	20e,26o
HF	0.9168[15]	$^1\Sigma_g^+$	1	H-1s,2s,2p, F-2s,2p,3s,3p	8e,17o
SiH_3F	1.6001*	$^1A_1$	6	H-1s,2s,2p, Si-3s,3p,4s,4p	14e,27o
CH_3F	1.3646[15]	$^1A_1$	2	C,F,2s,2p,3s,3p	14e/23o
XeF_2	1.9684*	$1\Sigma_g^+$	25	Xe-5s,5p,6s,6p, F-2s,2p,3s,3p	22e,35o

* Geometry optimized at the PBE0 level with the Sapporo-TZP basis.[18]

Table 6: Binding energy of some of the computed molecules, in Kcal/mol.

Molecule	D_E Exp.	D_E Calc.
H_2	109.5[19]	108.0
C_2	145.3	148.3
N_2	228.5	228.6
O_2	120.1[20]	117.4
F_2	38.3[19]	33.0
S_2	102.5	-
Cl_2	58.0	-
Br_2	-	-
Cu_2	47.7[21]	29.0
Ag_2	38.3[21]	23.3
Ag_2*	38.3[21]	30.3
Au_2*	52.8[21]	42.0

* With scalar relativistic corrections.

scalar effects were applied. All the electronic structure calculations were performed using PySCF[27].

Promolden[28] was used to obtain the atomic overlap matrices and the interacting quantum atoms (IQA) quantities. IQA integrations were performed using β-spheres with radii between 0.1 and 0.3 bohr. Restricted angular Lebedev quadratures with 3074 points and 451 points Gauss-Chebyshev mapped radial grids were used inside the β-spheres, with L expansions cut at $l = 8$. Outside the β-spheres, extended 5810-point Lebedev, 551 mapped radial point Gauss-Legendre quadratures, and L expansions up to $l = 10$ were selected. Electron distribution functions were obtained with the in-house code EDF[29] and the natural adaptive orbitals with denmat[30], another in-house code.

3.1 Difluorine

Table 8 shows the multireference data in F_2. At $R \approx 4$ Å the atomic limit is basically recovered. The deformation energy at equilibrium is 0.0782 au, very similar to the value obtained at the simple CAS level commented in the main text. This 49 kcal/mol deformation has to be compared with that in H_2 from a FCI calculation, which is about 8 kcal/mol per H atom. Notice

Table 7: Relevant real space parameters for the plausible CSB interaction in some of the compounds studied. Total value of δ, main components of the CSB interaction energy, number of eigen-contributions to δ, n, and value of the dominant eigenvalue, δ_i. Some selected IQA data are also presented. Atomic units used throughout.

Molecule	δ	$E_{\rm cov}$	$E_{\rm ion}$	n	δ_i
H_2	0.8474	-0.2388	0.0417	1	0.8321
C_2	1.8119	-0.5374	0.1419	4	0.6732
N_2	2.0057	-0.7025	0.2276	3	0.7836
$NH_2{-}NH_2$	1.1981	-0.3482	0.0460	1	0.8190
O_2	1.5493	-0.5115	0.1447	3	0.7185
HO−OH	0.9455	-0.2971	0.0286	1	0.7260
F_2	0.8854	-0.2594	0.0503	1	0.6125
S_2	1.6503	-0.3977	0.0620	3	0.7344
Cl_2	1.1522	-0.2776	0.0455	1	0.7541
Br_2	1.1144	-0.2387	0.0316	1	0.7335
Cu_2	1.0558	-0.1710	0.0037	1	0.7885
Ag_2	1.2046	-0.1667	0.0022	1	0.9631
Ag_2*	1.1877	-0.1739	0.0036	1	0.9338
Au_2*	1.5043	-0.2271	0.0100	1	0.9904
$Hg_2{}^{+}$*	1.2143	-0.1792	0.1542	1	0.9670

* With scalar relativistic corrections.

A-B groups	T^A	T^B	E^A_{self}	E^B_{self}	E^{AB}_{int}	$E_{\rm cov}$	$E_{\rm ion}$	Q^A	Q^B
$CH_3{-}F$	100.0784	39.4115	-99.4460	-39.3142	-0.6547	-0.2614	-0.3933	-0.7164	0.7169
$SiH_3{-}F$	100.0891	290.5504	-99.5219	-290.2868	-0.7145	-0.1443	-0.5702	-0.9020	0.9025
XeF−F	7229.8926	99.8638	-7231.1413	-99.5210	-0.5418	-0.1864	-0.3554	1.3802	-0.6904

A-B groups	T^A	E^A_{self}	E^{AB}_{int}	$E_{\rm cov}$	$E_{\rm ion}$	V^{intra}_{ee}	V^{inter}_{ee}
H_2	0.5866	-0.4876	-0.1971	-0.2388	0.0417	0.1515	0.2867
C_2	37.8706	-37.6630	-0.3956	-0.5375	0.1419	13.5090	13.2890
C-C^b, C_5H_6	37.8529	-37.5228	-0.0765	-0.1091	0.0326	14.4025	11.0876
N_2	54.6448	-54.4021	-0.4749	-0.7026	0.2277	20.6203	20.1699
$NH_2{-}NH_2$	55.7798	-55.6221	-0.3022	-0.3483	0.0461	27.5177	24.8703
O_2	75.0063	-74.8178	-0.3668	-0.5115	0.1447	29.1182	25.2505
HO−OH	75.6147	-75.4757	-0.2685	-0.2971	0.0286	33.2100	26.5017
F_2	99.5883	-99.4803	-0.2089	-0.2602	0.0513	39.9570	28.8515
S_2	397.8323	-397.4808	-0.3357	-0.3977	0.0620	152.9100	69.0588
Cl_2	459.8126	-459.4931	-0.2320	-0.2776	0.0456	176.0752	74.7267
Br_2	2571.6871	-2572.3995	-0.2071	-0.2387	0.0316	1010.6629	280.8390
Cu_2	1638.1732	-1638.9298	-0.1673	-0.1710	0.0038	651.1557	199.4370
$Ag_2{}^*$	-	-	-0.1702	-0.1739	0.0037	2018.2755	461.1527
Au_2	28037.8885	-14796.6130	-0.2171	-0.2272	0.0100	7061.8686	1334.6029
$Hg_2{}^{+2}$	29308.2546	-15051.2177	-0.0250	-0.1792	0.1542	7247.0955	1227.1356

* With relativistic corrections.

that all quantities evolve smoothly with distance. Covalent parameters are typical of a single bond, with a delocalization index at equilibrium close to that in dihydrogen. The EDF evolves as shown in Fig. 3. Only one electron pair is clearly being exchanged during bond formation and, at equilibrium the distribution is that of a normal correlated link. δ^{AB} shows a very shallow inflection point close to $R = 1.7$ Å with $\delta \approx 0.5$. This has been suggested as a measure of bond formation.[31] In this sense, difluorine reaches equilibrium soon after bond formation, as expected from a proto-bond. At variance with H_2 and other full-bonds, E_{self} displays an exponential-like behavior with decreasing distance, with no clear hint of the plateau that is usually found. E_{int} displays a minimum which is extrapolated to occur at about $R \approx 1.15$ Å, a much shorter distance than the equilibrium value. This points again to the large E_{self} as the reason behind the anomalously large R_e. As evidenced throughout this paper, this is linked to the LPBWE. We have also performed a CCSD(T) calculation with the aug-cc-pVTZ basis set at the experimental[15] geometry. This provides an improved binding energy of -36.4 kcal/mol. The IQA data do not change appreciably. The total DI decreases slightly to 0.8763. $E^{AB}_{clas} = 0.0516$ au remains almost constant, so it is the covalent contribution which accounts for the extra binding, increasing to $E^{AB}_{cov} = -0.2667$ au. Notice that the proto-bond character of the F-F link can also be sensed through other real space properties, like the localization or spread tensor (LT).[32] The LT of difluorine shows a considerably large peak which is usually associated to a bond-breaking process.

3.2 Dioxygen

Tables 9 and 10, together with Fig. 4 summarize the IQA and EDF results for dioxygen. The deformation energy of each O atom is larger than in F_2, 62 kcal/mol, but dioxygen is a clearly double-bonded system with a considerably smaller R_e. E_{def} of each F atom at $R = 1.20$ Å is larger than the value reported in O_2 by 18 kcal/mol. A second clear difference is found in the evolution of E_{def} with distance. A very clear shoulder is found in dioxygen, with two inflection points at about 2.1 and 1.4 Å. Thus a continuous change from the well-known behavior of E_{def} in full-bonded systems like H_2 or N_2, in which E_{def} shows a maximum and a minimum toward the exponential behavior of difluorine passing through the shoulder in dioxygen is observed. A minimum in V^{AA}_{ee} is also found. The covalent energy in the O_2 molecule is characteristic of a double bonded system, with δ considerably larger than

Table 8: Some IQA quantities in F_2. Distances in Å energies in au.

R	T	E^A_{self}	V^{AA}_{ee}	V^{AB}_{ee}	E^{AB}_{int}	E^{AB}_{cov}	E^{AB}_{clas}	δ^{AB}
1.20	99.8512	-99.4191	50.6462	33.2515	-0.2588	-0.3969	0.1381	1.1297
1.30	99.6874	-99.4460	50.3718	31.1712	-0.2409	-0.3264	0.0854	1.0164
1.41	99.5741	-99.4681	50.1455	29.0871	-0.2091	-0.2594	0.0503	0.8854
1.50	99.5218	-99.4816	50.0186	27.6052	-0.1806	-0.2140	0.0334	0.7789
1.60	99.4901	-99.4945	49.9164	26.0684	-0.1474	-0.1688	0.0214	0.6574
1.70	99.4788	-99.5054	49.8490	24.6695	-0.1167	-0.1307	0.0140	0.5401
1.80	99.4806	-99.5141	49.8100	23.3998	-0.0906	-0.0999	0.0093	0.4341
1.90	99.4872	-99.5220	49.7842	22.2323	-0.0682	-0.0748	0.0065	0.3402
2.00	99.4966	-99.5279	49.7716	21.1692	-0.0509	-0.0555	0.0046	0.2633
2.20	99.5130	-99.5360	49.7617	19.3022	-0.0275	-0.0301	0.0026	0.1540
2.40	99.5235	-99.5406	49.7597	17.7259	-0.0148	-0.0164	0.0015	0.0898
2.60	99.5294	-99.5431	49.7601	16.3840	-0.0081	-0.0091	0.0010	0.0536
2.80	99.5324	-99.5445	49.7601	15.2279	-0.0045	-0.0052	0.0006	0.0326
3.00	99.5339	-99.5453	49.7601	14.2231	-0.0025	-0.0030	0.0004	0.0204
3.20	99.5346	-99.5457	49.7601	13.3419	-0.0014	-0.0018	0.0003	0.0131
3.40	99.5349	-99.5460	49.7599	12.5629	-0.0008	-0.0011	0.0002	0.0086
3.60	99.5352	-99.5461	49.7599	11.8696	-0.0005	-0.0007	0.0001	0.0059
3.80	99.5352	-99.5462	49.7599	11.2484	-0.0003	-0.0004	0.0001	0.0042
4.00	99.5354	-99.5463	49.7600	10.6889	-0.0002	-0.0003	0.0001	0.0031

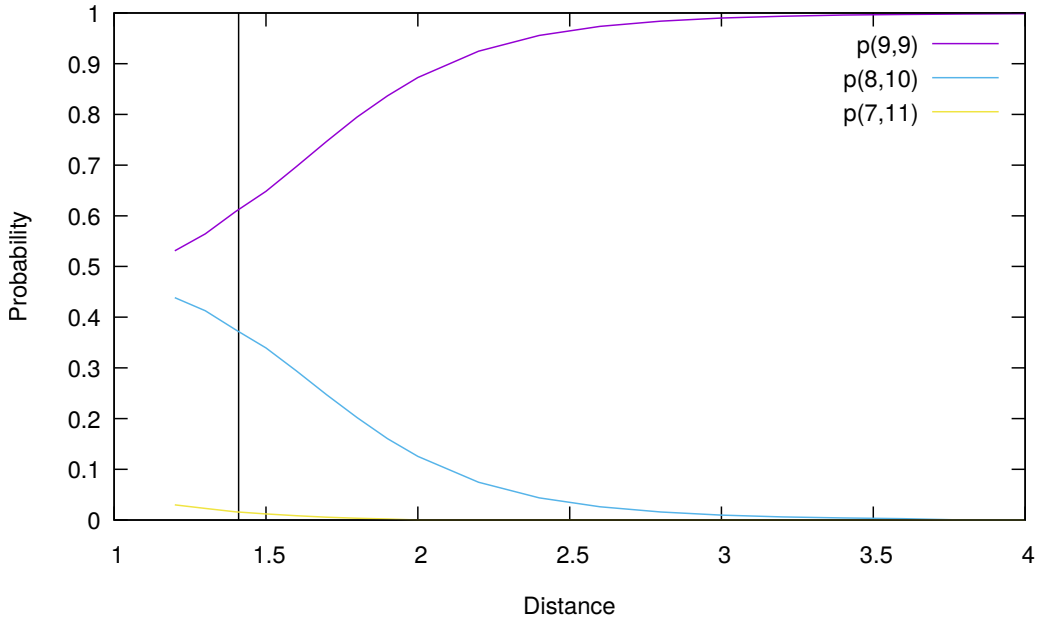

Figure 3: Evolution of the EDF in F_2. The weight of the ionic structures has been multiplied by a factor of two for convenience

Table 9: Some IQA quantities in O_2. Distances in Å energies in au.

R	T	E^A_{self}	V^{AA}_{ee}	V^{AB}_{ee}	E^{AB}_{int}	E^{AB}_{cov}	E^{AB}_{clas}	δ^{AB}
1.10	75.2365	-74.7991	37.6474	27.6547	-0.3802	-0.6140	0.2338	1.7044
1.21	75.0063	-74.8178	37.2984	25.7620	-0.3668	-0.5115	0.1447	1.5493
1.30	74.8848	-74.8274	37.0670	24.3119	-0.3407	-0.4360	0.0953	1.4188
1.40	74.8046	-74.8337	36.8766	22.9053	-0.3062	-0.3666	0.0603	1.2841
1.50	74.7577	-74.8388	36.7315	21.6277	-0.2688	-0.3069	0.0381	1.1532
1.60	74.7351	-74.8430	36.6275	20.4685	-0.2320	-0.2559	0.0239	1.0265
1.70	74.7307	-74.8475	36.5571	19.4094	-0.1964	-0.2114	0.0150	0.9001
1.80	74.7418	-74.8530	36.5170	18.4387	-0.1623	-0.1718	0.0095	0.7711
1.90	74.7666	-74.8598	36.5046	17.5450	-0.1295	-0.1356	0.0061	0.6367
2.00	74.8019	-74.8686	36.5145	16.7166	-0.0983	-0.1023	0.0040	0.4986
2.20	74.8726	-74.8960	36.5498	15.2377	-0.0494	-0.0517	0.0022	0.2683
2.40	74.8968	-74.9056	36.5629	13.9992	-0.0266	-0.0279	0.0012	0.1538
2.60	74.9029	-74.9105	36.5628	12.9450	-0.0156	-0.0164	0.0007	0.0967
2.80	74.9044	-74.9132	36.5602	12.0352	-0.0096	-0.0101	0.0004	0.0645
3.00	74.9048	-74.9148	36.5580	11.2425	-0.0061	-0.0064	0.0003	0.0449
3.20	74.9050	-74.9158	36.5568	10.5467	-0.0040	-0.0042	0.0002	0.0327
3.40	74.9052	-74.9163	36.5562	9.9311	-0.0027	-0.0029	0.0001	0.0249
3.60	74.9053	-74.9167	36.5557	9.3828	-0.0020	-0.0021	0.0001	0.0199
3.80	74.9054	-74.9169	36.5555	8.8916	-0.0014	-0.0015	0.0000	0.0166
4.00	74.9054	-74.9170	36.5555	8.4490	-0.0011	-0.0012	0.0000	0.0144
4.20	74.9054	-74.9171	36.5554	8.0483	-0.0009	-0.0010	0.0000	0.0130
4.40	74.9055	-74.9171	36.5554	7.6838	-0.0008	-0.0008	0.0000	0.0121
4.60	74.9055	-74.9172	36.5554	7.3508	-0.0007	-0.0007	0.0000	0.0114
4.80	74.9055	-74.9172	36.5555	7.0454	-0.0006	-0.0006	0.0000	0.0110

Table 10: Relevant EDF structures in O_2

Dist	(8,8)	(7,9)	(6,10)
1.10	0.4256	0.2435	0.0421
1.21	0.4482	0.2402	0.0345
1.30	0.4702	0.2355	0.0282
1.40	0.4978	0.2285	0.0222
1.50	0.5285	0.2184	0.0169
1.60	0.5641	0.2052	0.0125
1.70	0.6051	0.1883	0.0089
1.80	0.6525	0.1674	0.0062
1.90	0.7071	0.1425	0.0040
2.20	0.8712	0.0635	0.0000
2.40	0.9254	0.0368	0.0000
2.60	0.9531	0.0231	0.0000
2.80	0.9689	0.0153	0.0000
3.00	0.9784	0.0106	0.0000
3.20	0.9845	0.0076	0.0000
3.40	0.9883	0.0056	0.0000
3.60	0.9908	0.0044	0.0000
3.80	0.9924	0.0036	0.0000
4.00	0.9935	0.0030	0.0000
4.20	0.9942	0.0027	0.0000
4.40	0.9947	0.0025	0.0000
4.60	0.9950	0.0023	0.0000
4.80	0.9952	0.0022	0.0000

Table 11: Laplacian of the density for the asymmetric (A≠B) and symmetric molecules (A=B) at the bond critical point. Data in au.

Molecule	$\nabla^2\rho$(bcp)	Molecule	$\nabla^2\rho$(bcp)
CH_3F(C−F)	0.0582	H_2	-1.3676
LiOH(Li−O)	0.6480	C-C^b C_5H_6	0.1556
SiH_3F(Si−F)	1.1087	N_2	-3.1734
XeF_2(Xe−F)	0.2418	N_2H_4(N−N)	-0.5212
		O_2	-0.8396
		H_2O_2(O−O)	0.0356
		F_2	0.4964
		S_2	-0.3082
		Cl_2	-0.0841
		Br_2	-0.0375
		Cu_2	0.2352
		Ag_2	0.1813
		Au_2	0.2352
		Hg_2^{+2}	0.0960

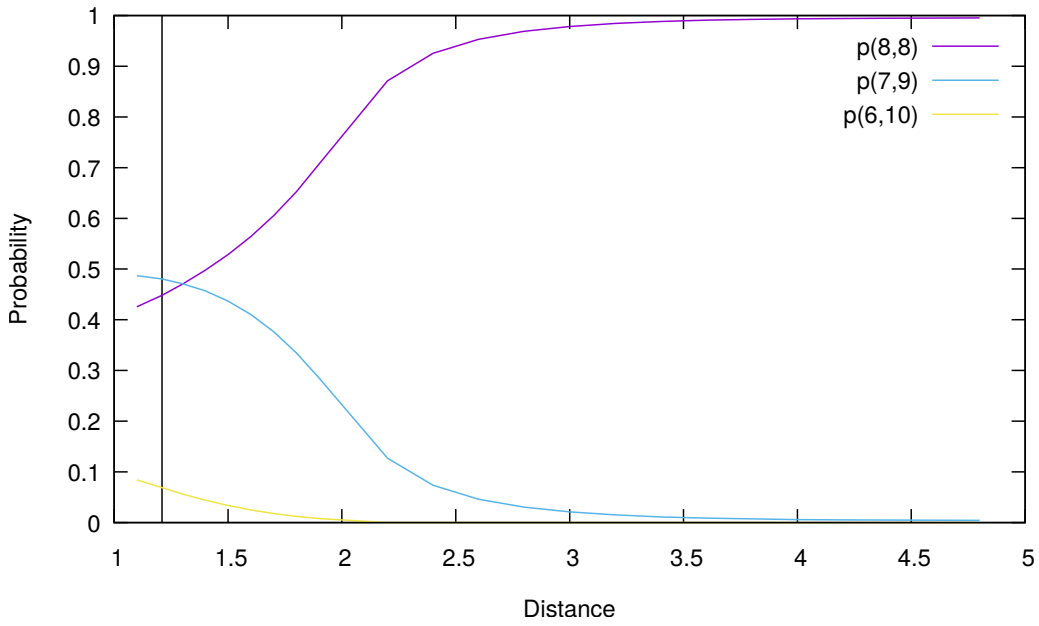

Figure 4: Evolution of the EDF in O_2. The weight of the ionic structures has been multiplied by a factor of two for convenience

1. The EDF shows clearly that the 0.5 intersection of the one-electron exchanges occurs at a distance larger than equilibrium, a notorious landmark of multiple bonding. Notice that the laplacian at the bond critical point is largely negative, as shown in Table 11.

3.3 Some transition metal diatomics

CSB has also been invoked to appear in many TM diatomics like Cu_2, Ag_2 and Au_2. As shown in Table 7, in all these systems the E_{cov} values are typical of rather standard covalent bonds, and the main eigencontribution to δ is only slightly low in dicopper. Relativistic effects have been gauged in Ag_2 through the X2C[25] approach. As the Table uncovers, these effects do not alter the bonding analysis significantly in Ag_2, but play a significant role in gold an mercury.

In the X2C approach, the electronic and positronic states are decoupled from the one electron Dirac equation

$$\begin{pmatrix} \hat{V} & c(\vec{\sigma}\cdot\vec{p}) \\ c(\vec{\sigma}\cdot\vec{p}) & \hat{V}-2c^2 \end{pmatrix}\begin{pmatrix} \phi^L \\ \phi^S \end{pmatrix} = E\begin{pmatrix} \phi^L \\ \phi^S \end{pmatrix} \tag{22}$$

where ϕ^L and ϕ^S are the large and small component of the four-component Dirac spinor, $\vec{p}$ is the standard momentum operator, $\vec{\sigma}$ the vector of Dirac matrices and $\hat{V}$ is the external potential. The Dirac equation is represented in terms of a kinetically balanced basis set[33], which yields the equation

$$\begin{pmatrix} \hat{V} & \hat{T} \\ \hat{T} & \frac{1}{4c^2}\hat{W}-\hat{T} \end{pmatrix}\begin{pmatrix} \phi^L \\ \phi^S \end{pmatrix} = E\begin{pmatrix} \hat{S} & 0 \\ 0 & \frac{1}{2c^2}\hat{T} \end{pmatrix}\begin{pmatrix} \phi^L \\ \phi^S \end{pmatrix} \tag{23}$$

where $\hat{S}$,$\hat{T}$,$\hat{V}$ are standard operators over spinors and $\hat{W}$ is a relativistic operator with matrix elements given by

$$W_{\mu\nu} = \langle\chi_\mu|(\vec{\sigma}\cdot\vec{p})\hat{V}(\vec{\sigma}\cdot\vec{p})|\chi_\nu\rangle \tag{24}$$

The four-component Hamiltonian in its matrix form can be block-diagonalized using a single matrix transformation

$$U^\dagger DU = \begin{pmatrix} h_+ & 0 \\ 0 & h_- \end{pmatrix} \tag{25}$$

$$D = \begin{pmatrix} V & T \\ T & \frac{1}{4c^2}W-T \end{pmatrix} \tag{26}$$

so that the electrons-only two-component equation is,

$$h_+C^{2c} = ESC^{2c}. \tag{27}$$

In the X2c one- electron scheme, or X2C-1e, h_+ is combined with untransformed two-electron interactions for subsequent Hartree-Fock and electron-correlated calculations. This scheme possesses the computational advantage that no relativistic two-electron integrals are required, while the underlying approximation is equivalent to the neglect of picture-change effects for the two-electron interactions. Furthermore, since only the W matrix is spin-dependent, spin separation for X2c-1e can be achieved by applying the Dirac identity to W

$$W_{\nu\mu} = W^{SF}_{\nu\mu} + W^{SO}_{\nu\mu} \tag{28}$$

$$W^{SF}_{\nu\mu} = \langle\chi_\nu|\vec{p}\cdot(\hat{V}\vec{p})|\chi_\mu\rangle \tag{29}$$

$$W^{SO}_{\nu\mu} = \langle\chi_\nu|i\vec{\sigma}\cdot(\vec{p}\times\hat{V}\vec{p})|\chi_\mu\rangle \tag{30}$$

the spin free version of X2c-1e which is used in this work is obtained by leaving out W^{SO}, the spin-orbit one electron term, from 23 at the beginning of the procedure. The decoupling transformation matrix U obtained during the Hamiltonian construction procedure is necessary for a later picture-change transformation of any monoelectronic property integral, like the density operator. The neglect of picture-change introduces errors in the electron density near the nucleus and small or negligible ones in the valence region that dominate the contructuction of the interatomic surface. Thus if one constructs the density in the usual way neglecting the transformation, the error is very small. Moreover as in this case the systems are homodiatomic, symmetry rules enforce the surface at the bisection plane between both nucleus, which is the surface obtained in the calculation. The atomic overlap matrices (AOM) are also affected by this error also only near the nuclei, but we expect that these zones do not contribute to bonding or other properties derived from AOMs. Otherwise n-th order matrices are not affected by our approximations, so no error should be expected neither from the NAdOs nor the EDFs.

3.4 N_2H_4 and H_2O_2

Two other systems with well known LPBWE that have also been reported as CSB are hydrazine and hydrogen peroxide. As shown in Table 7 there is a very clear decrease in the first eigen-component of the delocalization index on going from hydrazine to hydrogen peroxide to difluorine that is followed by E_{cov}. The EDFs show a well-defined electron-pair bond. In N_2H_4, using the $NH_2{-}NH_2$ partition, we find $p(9,9) = 0.510$ and $p(8,10) = 0.227$. A second electron exchange is residual (with $p(11,7) = 0.017$). This leads to a rather standard link with $f = 0.02$. In $H_2O{-}OH_2$ the residual two-electron exchange is even less important ($p(11,7) = 0.012$) and the electron-pair gives $p(9,9) = 0.552$, $p(8,10) = 0.211$, corresponding to $f = 0.11$. We must recall that in F_2 $f = 0.22$. The laplacians at bcps follow the expected trends (Tab. 11) and become positive, although only slightly, in H_2O_2. Notice also that as we increase the importance of CSB, we simply move to more positively correlated, i.e. more dissociated, standard bonds. Importantly, we corroborate that the larger the CSB contribution, the smaller the pair fluctuation, in flagrant contradiction with the basic tenets of VB-CSB.

3.5 Polar CSB: HF, XeF_2, CH_3F and SiH_3F

Not only non-polar bonds have been related to CSB. Many other electron-pair links that include F, for instance, have been shown to display very large NOVB covalent-ionic resonance energies. Among them the HF, and particularly the SiH_3F molecules, as well as many of the C-F bonds of well-known organic moieties. SiH_3F is reported to display covalent chemical behavior,[12] with much larger static polarity, while the chemistry of CH_3F, which is expected to be less polar, is more typically ionic. As briefly discussed in the main text, our calculations show clear signs of proto-bonding situations in all these cases, in agreement with Sanderson's insight that uncovers LPBWE as an atomic feature.

The methyl–fluorine or silyl-fluorine interactions display relatively large covalent energies, -0.261 and -0.144 au, respectively. The net QTAIM charges of the fluorine follow the electronegativity differences, being equal to -0.716 and -0.902 au, in line with other very polar systems. This implies that the ionic energy contributions are also large, -0.393 and -0.571 au, respectively. However, by no means a big ionic energy, related to a static charge distortion, is to be directly related to the absence of pair-electron sharing. As noted in the main text, the delocalization indices are $0.896, 0.591$ for the C-F and Si-F links, and the EDF analysis shows two rather correlated bonds with $f = 0.22, 0.60$. We emphasize that in none of the compounds examined we have found negative correlation factors that would clearly signal a real space anomalous fluctuation of the pair density.

The hydrogen fluoride molecule is found to display one of the largest NOVB covalent-ionic resonance energies, about 85 kcal/mol.[12] The F QTAIM charge is -0.745 au, quite compatible with that in CH_3F given the similar electronegativities of H and C. Its covalent and ionic energies turn out to be $-0.136, -0.343$ au, respectively. The latter is similar to the value in CH_3F, but the former is almost half of the exchange-correlation energy in methylfluoride, a value compatible with a much smaller $\delta = 0.424$. This difference is due to the inability of H to provide more than one electron to the fluorine atom, a limitation that does not exist in C. An analysis of the EDF, with $p(0, 10) = 0.756$, $p(1, 9) = 0.233$ gives $f = 0.05$. It is interesting that the value of the Laplacian of the density at the bcp is extremely negative, $\nabla^2\rho(\boldsymbol{r}_{bcp}) = -4.319$ au, a fact that definitively shows that the connection between laplacians and CSB is not one to one.

XeF_2 does also display a rather polar link. The F QTAIM charge is -0.690

au, with $E_{cov} - 0.1864$ and $E_{ion} = -0.355$ au. The Xe-F delocalization index is large, 0.780, and the EDF shows clear indication of futher than single bonding, with non-negligible three-center contributions. If these are neglected, the XeF-F EDF displays a correlation factor $f \approx 0.20$.

3.6 [1.1.1]Propellane

We end the presentation with a brief discussion of propellane. Its bridge C-C bond has been described as CSB. It is definitely longer (1.596 versus 1.524 Å for the non-bridging links) than a standard single C-C bond. Only two non-equivalent C atoms exist: the bridging C's, C_b, and the non-bridging C's, C_{nb}. The former are negatively charged ($Q_b = -0.081$) and the latter wear a positive charge of about 0.042 au, being more deformed by about 50.8 kcal/mol than the bridging atoms. Aside from some multicenter features, for instance the non-bonded C_{nb}-C_{nb} DI is very large (about 0.086), the C_b-C_b $E^b_{cov} = -0.109$ au and $\delta^b = 0.410$. These values are to be compared with $E^{nb}_{cov} = -0.257$ au, $\delta^{nb} = 0.803$. Special care has to be taken with the interpretation of EDFs in cyclic systems. A full analysis (which will be presented elsewhere) shows a symmetric 2c,2e link with large f. The main NAdO for the C-C bridge is clearly σ-like, between two heavily hybridized functions, and $\nabla^2\rho = 0.155$ au at the C_b-C_b bcp. Fig. 5 shows the main NAdO of the system.

Figure 5: Critical points (with $\nabla^2\rho$) in propellane (left), together with the main bonding natural adaptive orbital (right, $\delta_i = 0.352$) for its bridging bond.

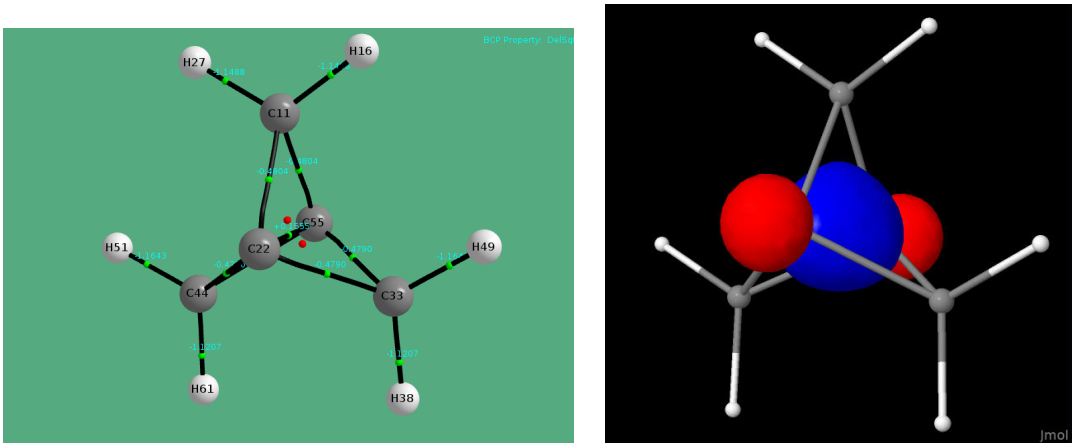

References

[1] R. F. W. Bader, *Atoms in Molecules*, Oxford University Press, Oxford, 1990.

[2] A. D. Becke and K. E. Edgecombe, *J. Chem. Phys.*, 1990, **92**, 5397.

[3] M. A. Blanco, A. M. Pendás and E. Francisco, *Journal of Chemical Theory and Computation*, 2005, **1**, 1096–1109.

[4] D. Menéndez-Crespo, A. Costales, E. Francisco and A. Martín Pendás, *Chem. Eur. J.*, 2018, http://dx.doi.org/10.1002/chem.201800979.

[5] E. Francisco, A. Martín Pendás and M. A. Blanco, *J. Chem. Phys.*, 2007, **126**, 094102–1–094102–13.

[6] A. Martín Pendás, E. Francisco and M. A. Blanco, *J. Chem. Phys.*, 2007, **127**, 144103.

[7] C. Outeiral, M. A. Vincent, A. Martín Pendás and P. L. A. Popelier, *Chem. Sci.*, 2018, **9**, 5517–5529.

[8] E. Francisco, A. Martín Pendás, M. García-Revilla and R. Álvarez Boto, *Comput. Theor. Chem.*, 2013, **1003**, 71–78.

[9] M. Menéndez, R. Álvarez Boto, E. Francisco and Á. Martín Pendás, *J. Comp. Chem.*, 2015, **36**, 833–843.

[10] A. Martín Pendás, E. Francisco and M. A. Blanco, *Phys. Chem. Chem. Phys.*, 2007, **9**, 1087–1092.

[11] A. Martín Pendás and E. Francisco, *Phys. Chem. Chem. Phys.*, 2018, **20**, 16231–16237.

[12] S. Shaik, D. Danovich, B. Silvi, D. L. Lauvergnat and P. C. Hiberty, *Chem. Eur. J.*, 2005, **11**, 6358–6371.

[13] A. Martín Pendás and E. Francisco, *Phys. Chem. Chem. Phys.*, 2018, **20**, 12368–12372.

[14] J. L. Casalz-Sainz, J. M. Guevara-Vela, E. Francisco, T. Rocha-Rinza and Á. Martín Pendás, *ChemPhysChem*, 2017, **18**, 3553–3561.

[15] *WebBook, NIST Standard Reference Database Number 69*, National Institute of Standards and Technology, Gaithersburg MD, 20899, 2017.

[16] J. L. Jules and J. R. Lombardi, *J. Phy. Chem. A*, 2003, **107**, 1268–1273.

[17] G. Durand, F. Spiegelmann and A. Bernier, *Journal of Physics B: Atomic and Molecular Physics*, 1987, **20**, 1161.

[18] T. Noro, M. Sekiya and T. Koga, *Theoretical Chemistry Accounts*, 2012, **131**, 1–8.

[19] S. Shaik, P. Maitre, G. Sini and P. C. Hiberty, *Journal of the American Chemical Society*, 1992, **114**, 7861–7866.

[20] D. Danovich, C. Foroutan-Nejad, P. C. Hiberty and S. Shaik, *Journal of Physical Chemistry A*, 2018, **122**, 1873–1885.

[21] S. Radenković, D. Danovich, S. Shaik, P. C. Hiberty and B. Braïda, *Computational and Theoretical Chemistry*, 2017, **1116**, 195–201.

[22] J. E. Smith, B. Mussard, A. A. Holmes and S. Sharma, *Journal of Chemical Theory and Computation*, 2017, **13**, 5468–5478.

[23] S. Sharma, A. A. Holmes, G. Jeanmairet, A. Alavi and C. J. Umrigar, *Journal of Chemical Theory and Computation*, 2017, **13**, 1595–1604.

[24] A. A. Holmes, N. M. Tubman and C. J. Umrigar, *Journal of Chemical Theory and Computation*, 2016, **12**, 3674–3680.

[25] W. Kutzelnigg and W. Liu, *Journal of Chemical Physics*, 2005, **123**,.

[26] E. R. Sayfutyarova, Q. Sun, G. K. L. Chan and G. Knizia, 2017, 26.

[27] Q. Sun, T. C. Berkelbach, N. S. Blunt, G. H. Booth, S. Guo, Z. Li, J. Liu, J. McClain, S. Sharma, S. Wouters and G. K.-L. Chan, *The Python-based Simulations of Chemistry Framework (PySCF)*, http://arxiv.org/abs/1701.08223, 2017.

[28] A. Martín Pendás and E. Francisco, A QTAIM/IQA code (Available from the authors upon request).

[29] E. Francisco, A. M. Pendás and M. Blanco, *Computer Physics Communications*, 2008, **178**, 621 – 634.

[30] E. Francisco, *Denmat. A cumulant analysis code (Available from the authors upon request.)*.

[31] M. García-Revilla, P. L. A. Popelier, E. Francisco and A. Martín Pendás, *J. Chem. Theory Comput.*, 2011, **7**, 1704.

[32] O. Brea, M. E. Khatib, C. Angeli, G. L. Bendazzoli, S. Evangelisti and T. Leininger, *Journal of Chemical Theory and Computation*, 2013, **9**, 5286–5295.

[33] R. E. Stanton and S. Havriliak, *The Journal of Chemical Physics*, 1984, **81**, 1910–1918.